GEOPHYSICS, VOL. 77, NO. 2 (MARCH-APRIL 2012); P. M17–M26, 14 FIGS.
10.1190/GEO2011-0197.1

An effective crosswell seismic traveltime-estimation approach for quasi-continuous reservoir monitoring

Adeyemi Arogunmati[1] and Jerry M. Harris[2]

ABSTRACT

We present an iterative approach for quasi-continuous time-lapse seismic reservoir monitoring. This approach involves recording sparse data sets frequently, rather than complete data sets infrequently. In other words, it involves acquiring a completely sampled baseline data set followed by sparse monitor data sets at short calendar-time intervals. We use the term "sparse" to describe a data set that is a small fraction of what would normally be recorded in the field to reconstruct a high-spatial-resolution image of the subsurface. Each monitor data set could be as little as 2% of a single, complete conventional data set. The series of recorded time-lapse data sets is then used to estimate missing, unrecorded data in the sparse data sets. The approach was tested on synthetic and field crosswell traveltime data sets. Results show that this approach can be effective for quasi-continuous reservoir monitoring. Also, the accuracy of the estimated data increases as more sparse data sets are added to the time-lapse data series. Finally, a moving estimation window can be used to reduce computational effort for estimating data.

INTRODUCTION

Time-lapse monitoring projects are designed to observe changes in a reservoir over a period of time. This period often varies from a few months to a few years (e.g., Mathisen et al., 1995; Landrø et al., 1999; Arts et al., 2004). With increased interest in CO_2 sequestration in geologic reservoirs (Benson et al., 2005), time-lapse seismic monitoring will help to ensure safe storage. Monitoring stored CO_2 in geologic reservoirs may be needed for the site license, reservoir performance assessment, and leak detection. During the injection phase, when the reservoir pressure may be changing, faults may be reactivated, creating flow conduits or leaks that can lead to loss on containment. Fault reactivation could be of concern in many time-lapse projects (e.g., Wiprut and Zoback, 2000; Røste et al., 2007). Early detection of leaks through such conduits is more likely if a quasi-continuous monitoring program is in place. Also, hydrocarbon reservoirs will benefit from an effective quasi-continuous seismic monitoring strategy to ensure efficiency and timely management decisions.

Conventional time-lapse monitoring scenarios require significant time to acquire and process a full 3D seismic data volume (e.g., Lumley, 2001; Clarke et al., 2005). This time will be exacerbated by implementation of a quasi-continuous monitoring strategy that uses conventional data volumes. In this article, we investigate a data-estimation-based approach for quasi-continuous seismic monitoring (Harris, 2004; Harris et al., 2007). The central reasoning behind our approach is that we record a complete baseline survey data set followed by a series of sparse monitor data sets and estimate unrecorded or missing data from recorded data taken at earlier and later times. Smaller data-acquisition intervals result in better data-estimation constraints. The goal is quasi-continuous assessment of the subsurface reservoir, not real-time assessment.

If implemented, our approach would design the acquisition of smaller data sets more frequently. The recorded data volume might be on the order of 2% of what would be required by conventional strategies, depending on the frequency of the recording. Picking arrivals on sparse data sets may be somewhat difficult because the visual cue provided by long continuous arrivals is absent. A possible way around this difficulty is to use guide picks predicted using previously reconstructed velocity models. Another possibility is to use guide picks from the completely sampled baseline data set.

The proposed method can be made more efficient by the use of permanently installed sources and receivers. Some of the benefits of using permanently installed receivers are described in Landrø and Skopinseva (2008). These benefits include the opportunity for an improved time-lapse seismic signal. Several time-lapse monitoring

Manuscript received by the Editor 5 June 2011; revised manuscript received 3 December 2011; published online 24 February 2012.
[1]Presently BP America Inc., Houston, Texas, USA; formerly Stanford University, Department of Geophysics, Stanford, California, USA. E-mail: adeyemi.arogunmati@BP.com.
[2]Stanford University, Department of Geophysics, Stanford, California, USA. E-mail: jerry.harris@stanford.edu.

projects currently use permanently installed receivers. These include time-lapse projects at the Valhall field (Barkved et al., 2005), Clair field (Foster et al., 2008), and Chirag-Azeri fields (Foster et al., 2008). Repeated costs associated with redeployment of seismic data-acquisition equipment can be avoided.

Several techniques have been proposed for geophysical model construction from time-lapse sparse data. These include dynamic imaging techniques, for example, DynaSIRT (Santos and Harris, 2008), ensemble Kalman filter dynamic inversion (Quan and Harris, 2008), and temporal regularization joint inversion (Ajo-Franklin et al., 2005). DynaSIRT is a dynamic iterative reconstruction technique that uses weighted data from previous surveys together with the data from the time of interest to iteratively construct a geophysical model. On the other hand, dynamic inversion with ensemble Kalman filters updates the geophysical model using current sparse data. The joint inversion approach presented by Ajo-Franklin et al. (2005) relies on regularization in slow time to account for the data sparsity.

We believe quasi-continuous monitoring would benefit from a stochastic estimation approach, where statistics calculated from a training data set are used to estimate missing data. In our case, the training statistics could come from a completely sampled baseline data set. In particular, we investigate an autoregression technique involving the use of prediction error filters (PEFs) in estimating unrecorded traveltime data in a quasi-continuous time-lapse seismic monitoring scenario. Claerbout (2008) suggests a two-step approach for estimating missing data with PEFs. In the first stage, the PEF is estimated from the partially recorded data set (or training data); in the second stage, the missing data are estimated using the PEF and the partially recorded data. In our approach, the initial training data set is the full baseline data volume.

Li and Nowack (2004) show with examples that the spatial resolution of seismic tomography reconstruction from traveltime data can be improved if traveltimes extrapolated using PEFs to regions of low seismic ray coverage are included in the tomographic reconstruction. Our approach uses interpolation and extrapolation to improve the coverage because the proposed survey produces sparse coverage by design. We also use available data from previous surveys and later surveys in the missing data-estimation process. With the level of sparsity proposed with our approach, use of the baseline survey may prove to be inadequate for training statistics; therefore, we update the training statistics through use of the most recent completely sampled data. In other words, we implement a spatio-temporal data-estimation scheme. The method is explained in the following section, followed by synthetic and field examples that illustrate the efficiency of the proposed approach, then, finally, conclusions.

METHOD

Our data-estimation problem deals with quasi-continuous time-lapse seismic data that vary in space and calendar (or slow) time. We assume that a data set could be recorded fully or sparsely. We will represent the spatial domain with number subscripts and the slow time with number superscripts. In addition, the estimation problem also involves references to completely sampled data sets, which we will represent with the subscript c; partially sampled or sparse data sets, which we will represent with the subscript s; and unrecorded data sets, which we will represent with the subscript u. Using this nomenclature, the first complete survey $\mathbf{d}_c^1$ is

$$\mathbf{d}_c^1 = [\, d_1^1 \quad d_2^1 \quad d_3^1 \quad \dots \quad d_N^1 \,]^T, \tag{1}$$

where N is the number of list order samples. A complete data set is the sum of a sparse (recorded) data set and the unrecorded data set, i.e.,

$$\mathbf{d}_c^k = \mathbf{d}_s^k + \mathbf{d}_u^k, \tag{2}$$

where $\mathbf{d}_s^k$ is the sparsely recorded data at time k and $\mathbf{d}_u^k$ is the unrecorded data at time k. Rewriting equation 2 with an identity matrix gives

$$\mathbf{d}_c^k = \mathbf{S}\mathbf{d}_c^k + (\mathbf{I} - \mathbf{S})\mathbf{d}_c^k, \tag{3}$$

where we observe that

$$\mathbf{d}_s^k = \mathbf{S}\mathbf{d}_c^k, \tag{4}$$

$$\mathbf{d}_u^k = (\mathbf{I} - \mathbf{S})\mathbf{d}_c^k, \tag{5}$$

and $\mathbf{S}$ can be interpreted to be a data selection operator that selects which data are recorded from the otherwise complete data set.

If an "accumulated" data volume $\mathbf{a}_c^k$ of k time-lapse surveys is given as

$$\mathbf{a}_c^k = [\, \mathbf{d}_c^1 \quad \mathbf{d}_c^2 \quad \mathbf{d}_c^3 \quad \dots \quad \mathbf{d}_c^k \,]^T, \tag{6}$$

then also

$$\mathbf{a}_c^k = \mathbf{a}_s^k + \mathbf{a}_u^k, \tag{7}$$

where $\mathbf{a}_s^k$ is the accumulated sparse data volume up to time k and $\mathbf{a}_u^k$ is the accumulated unrecorded data volume up to time k. To estimate the unrecorded data, we apply an autoregressive algorithm to $\mathbf{a}_s^k$. The autoregressive data-estimation algorithm requires an assumption of ergodicity — namely that the statistics of the seismic data points in space are equivalent to the statistics of one repeatedly measured data point. Though not always valid in practice, this assumption is fundamental to estimation using autoregression. Because the extent to which this assumption is valid is likely to be small, we have chosen to use the nonstationary (slow time) formulation of the autoregressive data-estimation method.

The goal of our estimation problem is to obtain an estimate of the accumulated, completely sampled data volume $\tilde{\mathbf{a}}_c^k$ using the accumulated recorded sparse data volume $\mathbf{a}_s^k$ up to and including time k., i.e.,

$$\tilde{\mathbf{a}}_c^k = \mathbf{a}_s^k + \tilde{\mathbf{a}}_u^k, \tag{8}$$

where $\tilde{\mathbf{a}}_u^k$ is the estimate of the accumulated unrecorded data at time k. We use the nonstationary form (Margrave, 1998) of the autoregression model (Jain, 1989) to compute $\tilde{\mathbf{a}}_u^k$.

Autoregression models have been applied in many data prediction and data-estimation problems (e.g. Takanami and Kitagawa, 1991). A summary of the autoregressive model is given in Appendix A. We use a PEF, also reviewed in Appendix A. Claerbout (1998) suggests a two-stage process for estimating missing data using the PEF. In the first stage, the optimal PEF for the

available data is estimated. In the second stage, the estimated PEF is then used to estimate the missing data.

Implementation

Estimating the optimal PEF could be done, using the incomplete sparse data with the missing data masked (Claerbout, 1998, 2008) or by using a training data set (Curry, 2008). The estimation procedure for time-lapse monitoring assumes there exists a completely sampled baseline data set. Following the two-step approach suggested by Claerbout (2008), we use this complete baseline data set for training statistics and to make the initial estimate of the PEF. We then use an iterative strategy to obtain an estimate of the unrecorded data at each time k. The strategy begins with estimating the initial nonstationary PEF using the training data set. We use the completely sampled baseline data set as the initial estimate of the PEF to be used for each time instance.

In the second iteration, the resulting estimated accumulated complete data set from the first iteration is then used to reestimate the nonstationary PEF. This PEF is an improvement over the first estimate of the PEF obtained because new sparse measurements are used. The updated PEF is then used to reestimate the accumulated unrecorded data set. This process is repeated until convergence is reached. In other words, we continue the iterations until changes in the estimated PEF or estimated data are negligible.

The entire iterative process is repeated each time new sparse data sets are added to the accumulated volume. By repeating the process each time new data are available, previously estimated unrecorded data sets are reestimated. In effect, each additional sparse data set provides more data to further constrain the estimates of unrecorded data at previous times. The improvement in the previous estimates becomes negligible as the number of later sparse data sets increases.

SYNTHETIC CROSSWELL TRAVELTIME EXAMPLE

We use a synthetic baseline velocity model and changing models generated through flow simulation to simulate a quasi-continuous time-lapse monitoring scenario for a CO_2 storage site. Beginning with a baseline velocity model (Figure 1), we create 70 additional synthetic models representing the seismic velocity between two wells at two-week intervals over a period of 140 weeks, beginning, say, January 1, 1993. A CO_2 leak occurs after approximately 40 weeks into the CO_2 injection phase. We use a source and receiver configuration that mirrors a field configuration of a West Texas CO_2 enhanced oil recovery (EOR) pilot site (Figure 2), with 200 sources and 191 receivers. Source and receiver intervals are both 1.55 m. The depth interval of interest is about 300 m.

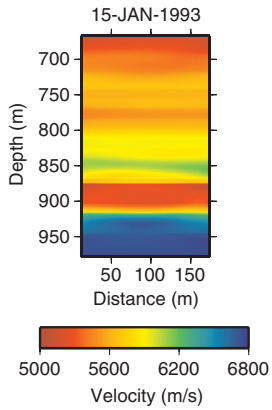

Figure 1. Synthetic baseline velocity model.

Conventional time-lapse monitoring

To represent conventional time-lapse monitoring, we use only two velocity models, with a time interval of 140 weeks between the baseline and monitor surveys. In other words, we use only the baseline and the seventieth time-lapse velocity model and record two full monitoring surveys. To simulate this, we compute first-arrival traveltimes for a crosswell geometry using the finite-difference method described in Hole and Zelt (1995). Figure 3

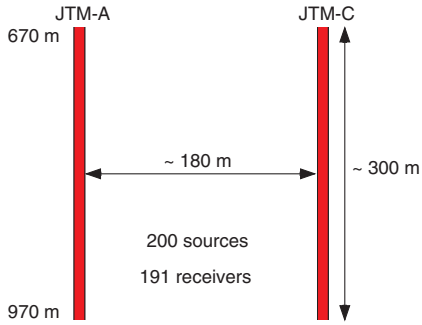

Figure 2. Crosswell data-acquisition configuration for the West Texas data set.

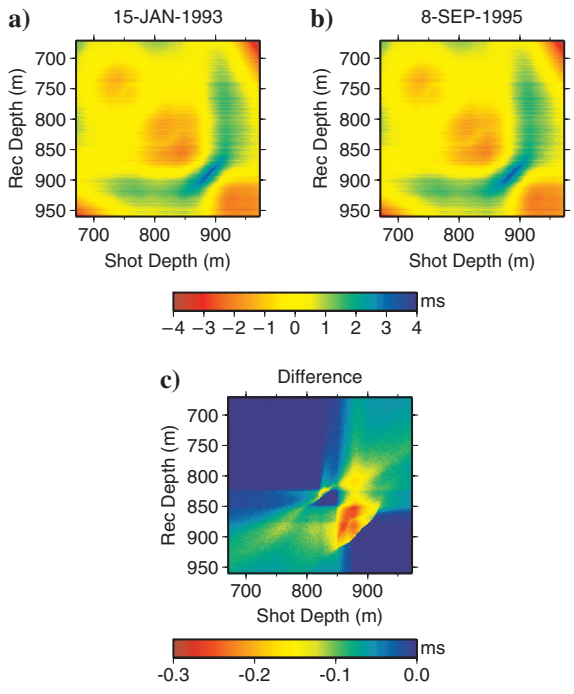

Figure 3. (a) Synthetic baseline traveltime data set. (b) Monitor traveltime data set for data set 70. (c) The difference between (a) and (b). The data shown in (a) and (b) have been reduced by a constant velocity of 5800 m/s.

shows the two computed baseline and time-lapse traveltime data sets. The traveltime data sets are displayed on a grid with the x- and y-axes represented by the shot and receiver depths, respectively.

To reconstruct the velocity models, we use the regularized tomography algorithm described in Zelt and Barton (1998). Each data set is inverted independently, and the difference between the reconstructed velocity model from the baseline data set and the reconstructed velocity model from the monitor data set gives the time-lapse velocity change. The true and reconstructed velocity-difference models are shown in Figure 4. The rms error shown in Figure 4 is the image error between 800 and 900 m depth, the location of the target reservoir where CO_2 was injected. Although the time-lapse velocity difference is well resolved, the leak is first detected long after it started, in week 140. In a real CO_2 sequestration project, such late detection could be problematic.

Quasi-continuous time-lapse monitoring

For each of the 70 time-lapse velocity models synthesized, we compute first-arrival traveltimes for a crosswell-seismic geometry. We use the same source and receiver configuration as the conventional example described in the previous section, which mirrors the configuration used in the West Texas field. We then subsample the synthetic data sets following the quasi-continuous monitoring strategy described. This is accomplished by discarding large portions of each data set.

Four groups of subsampled (sparse) data sets are created: 1%, 2%, 5%, and 10% of the original data volume. For comparison, we ensure that the accumulated data volumes of the subsampled data sets at the end of the two-year period are equal. This two-year period represents one complete recording cycle. For the 1% case, we sample 1% of each of the 70 synthetic data sets, discarding 99% of each data set; for the 2% case, we sample 2% of every other data set, discarding 98% of the data from alternating data sets and 100% of the others; for the 5% case, we sample 5% of every fifth data set, discarding 95% from every fifth data set and 100% of the others; and for the 10% case, we sample 10% of every tenth data set, discarding 90% from every tenth data set, and 100% of the others. Both random and regular sampling scenarios are tested. For the random sampling case, we tested data selection scenarios where all possible source and receiver locations for one complete conventional survey were used in each data-recording cycle and scenarios where there were repeated measurements at certain source and receiver locations. In the former case, all data points were used in each data-recording cycle; in the latter case, some data points were omitted in each data-recording cycle. The results presented in this paper are from the random-sampling-test scenario, where there was no repeated measurement in a recording cycle. It should be noted that similar conclusions can be made from the results obtained using regular sampling data sets.

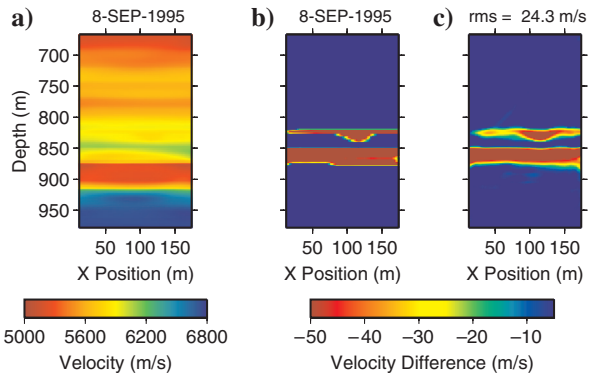

Figure 4. (a) The true velocity model after 140 weeks. (b) The true time-lapse velocity-difference model after 140 weeks. (c) The reconstructed velocity-difference model after 140 weeks. The injected CO_2 is well resolved, but only after 140 weeks.

Figure 5 shows selected true velocity-difference models alongside models reconstructed from complete synthetic traveltime data sets. These reconstructions are very good, as one would expect from complete time-lapse data sets. Clearly, the crosswell geometry is effective for identifying the leak if the survey is taken, but it does so at the expense of significantly larger data acquisition effort. Reconstructions from the sparse subsampled data sets produce geologically unreasonable models, showing significant artifacts. This is because the inverse or imaging problem is severely underdetermined with small sparse data sets, e.g., 5%. A first-order fix for a severely underdetermined problem is to reduce the number of model parameters estimated in the inverse problem. The consequence of this action is to reduce spatial resolution, e.g., increase the smallest model feature reconstructed.

Next, we construct time-lapse data volumes for use in quasi-continuous monitoring by concatenating data sets from different surveys in slow time. This produces a 3D traveltime volume. We then use the iterative PEF approach described in the previous section to estimate the missing, e.g., discarded, data. As the starting guess for the iterative process, we use the initial data set (baseline) and assume the traveltimes change slowly over the period to the first slow-time survey. We then estimate a PEF from the resulting time-lapse data volume and use this PEF to estimate the missing data. This process is repeated until convergence or until a tolerance measure is met. An example of complete and estimated data differences is shown in Figure 6. Although it is obvious in Figure 6 that the PEF

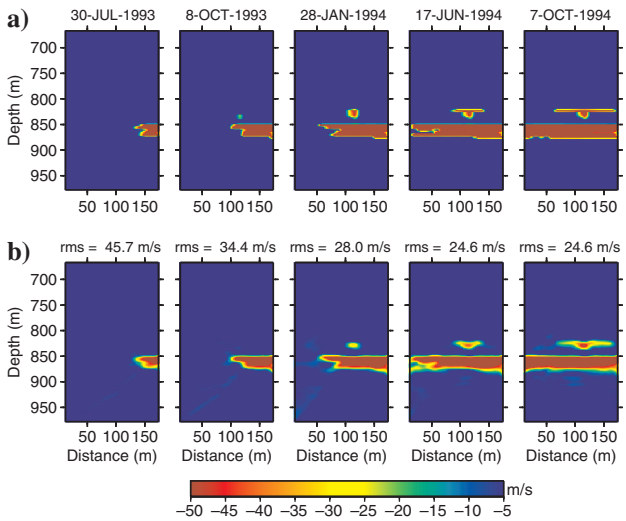

Figure 5. (a) Selected true synthetic velocity-difference models. The model dates are shown above each model. (b) Selected reconstructed velocity-difference models from complete true synthetic traveltimes. These represent the best images that can be reconstructed from the synthetic traveltimes. The model rms errors are shown above each reconstructed velocity model.

approach is effective in estimating missing data, this observation is quantitatively verified, as shown in Figure 7 where the rms errors are shown over a complete data-estimation cycle as new sparse data are incorporated. In Figure 7, N is the number of sparse time-lapse data sets (surveys) used in the estimation process. One key observation is that the errors are similar, regardless of the sparsity of data sets. This implies that the same level of model accuracy can be obtained with a smaller data size using the approach presented in this paper (i.e., by acquiring less data more frequently). In addition, by sampling more frequently, we increase the slow-time temporal resolution.

The error plots in Figure 8 illustrate that the accuracy of the reconstructed slowness models improves as the number of iterations increases. This shows a convergence toward the true model shown in Figure 7. Finally, we see a decrease in rms error as data volume increases, i.e., as more data are acquired, the accuracy of the estimated data increases. The improvement, however, decreases as more and more data are accumulated.

In Figures 7 and 8, it is obvious that after some time, adding new data sets does not improve the estimation error for previously estimated data sets. For these data sets, acceptable convergence has been reached. This implies that a smaller, moving estimation

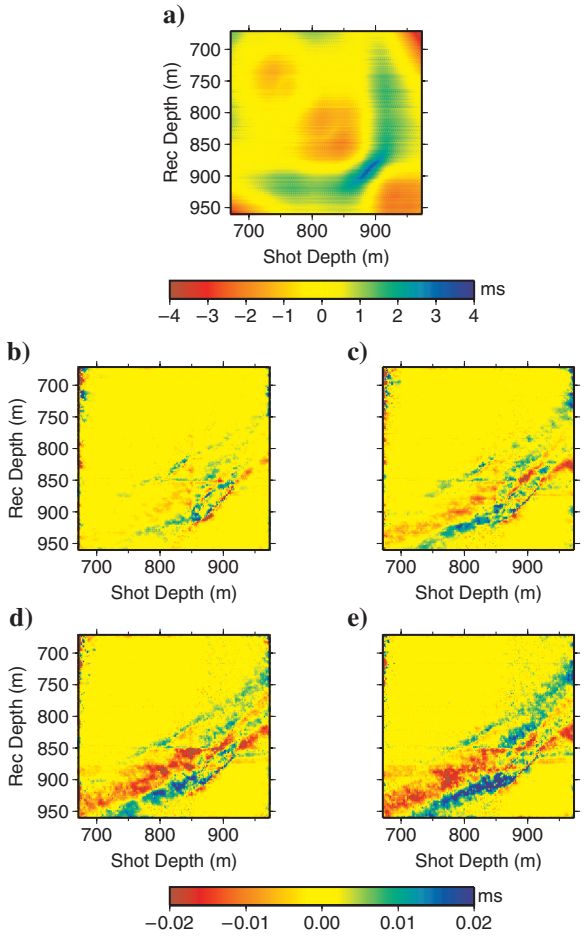

Figure 6. (a) A selected complete synthetic traveltime data set and the corresponding difference data sets for (b) 10% sparse + 90% estimated data, (c) 5% sparse + 95% estimated data, (d) 2% sparse + 98% estimated data, (e) 1% sparse + 99% estimated data.

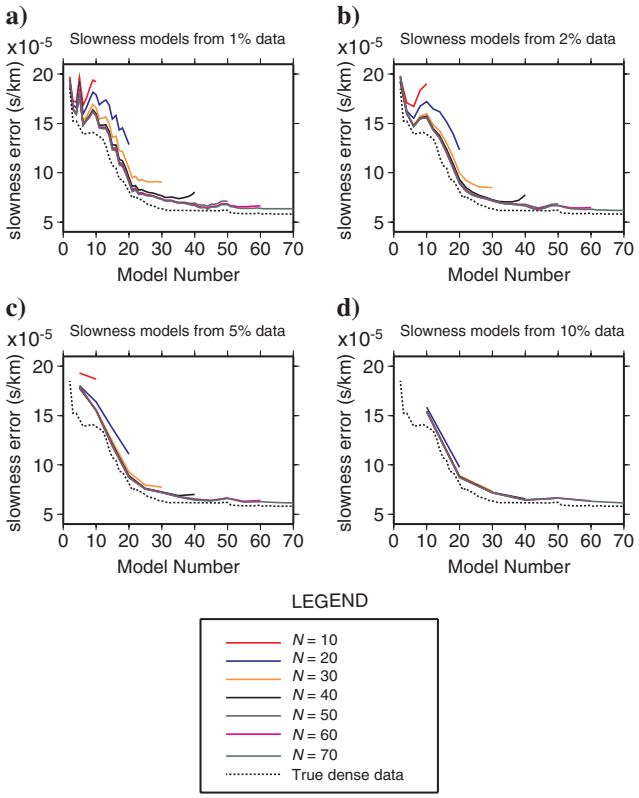

Figure 7. The rms error plots of the reconstructed slowness models from estimated traveltime data sets, grouped by the size of the original sparse data sets; only the third iteration results are shown. The dashed line in each plot shows the result obtained using complete data: (a) 1% sparse data, (b) 2% sparse data, (c) 5% sparse data, (d) 10% sparse data. The plots are color-coded by the number of sparse, time-lapse data sets N used in the estimation of missing data.

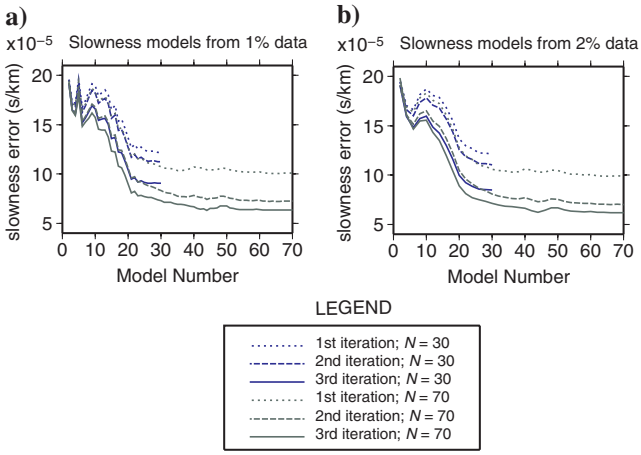

Figure 8. The rms error plots of the reconstructed slowness models from estimated traveltime data sets grouped by the size of the original sparse data sets, showing all three iteration results. Data are estimated using (a) 1% sparse data and (b) 2% sparse data. The plots are color-coded by the number of sparse, time-lapse data sets N used in the estimation of missing data.

window can be used instead of using and reestimating all data volumes at all times. If a moving estimation window is used, the first indication of abnormalities may warrant expanding the time window backward in time for confirmation. Also, a converged data set can be used instead of the baseline data set to train the initial PEF for the iterative process because we expect it to be more similar to the most recent data set than the baseline data set is.

To examine the benefits of calculating a new PEF when new sparse data sets are added, we reconstruct the synthetic velocity models using previously estimated PEFs and then compare them to the results obtained when a new PEF is recalculated. In Figure 9, we show rms slowness errors obtained after the second and third iterations when the estimated traveltime data used in the reconstruction process are from 1% sparse data. The rms errors are lowest when the PEF used is calculated from a time-lapse data volume that includes all available data sets. In addition, the rms errors of the slowness model reconstructed from the data estimated using the PEF calculated from the first 10 data sets are worse than those using the PEF calculated from the first 20 data sets, and so on. The errors are seen to decrease with data completeness, implying convergence. This shows that as the reservoir properties evolve and more data are acquired, the estimated PEF gets closer to the true PEF.

In Figure 10, we compare a series of reconstructed velocity models using the estimated data sets with different degrees of sparsity. The selected velocity models represent the period around the time the leak began, i.e., velocity model 21. Because the slow-time sampling rate of the reconstructed velocity models from data estimated using 2% sparse data is higher than the sampling rates of the 5% and 10% sparse data, the leak is detected much earlier in the 2% case than in the 5% or 10% cases. In addition, because the data sparsity of the 1% case is very high, the leak is not detected early. This shows that using the appropriate data sparsity is as important as obtaining the right slow-time resolution. Although this PEF approach to data estimation is effective, the fact that the error shrinks as more data sets are acquired gives it the property of delayed accuracy. Because the data are estimated from future and past data, accuracy increases as more data are acquired.

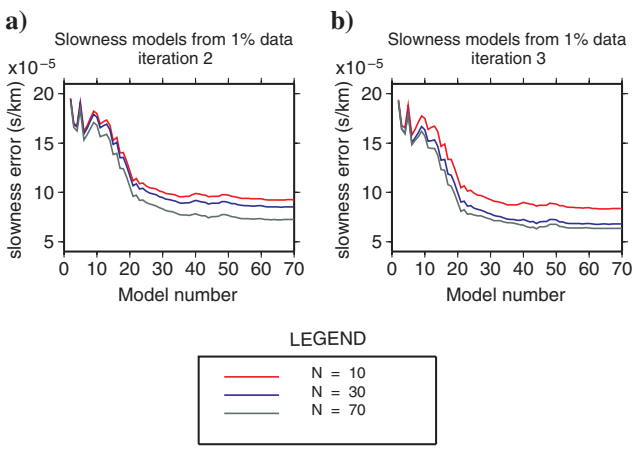

Figure 9. The rms error plots of the reconstructed velocity models from estimated traveltime data sets. The plots are color-coded by the number of data sets used in estimating the PEFs applied (a) after the second iteration and (b) after the third iteration.

RESERVOIR MONITORING AT THE MCELROY FIELD

A conventional time-lapse monitoring project was conducted in the McElroy field in West Texas with crosswell acquisition geometry. The baseline data set was acquired in 1993, and a monitor data set was acquired in 1995 (Harris et al., 1995; Lazarotos and Marion, 1997). Selected shot gathers are shown in Figure 11. The project

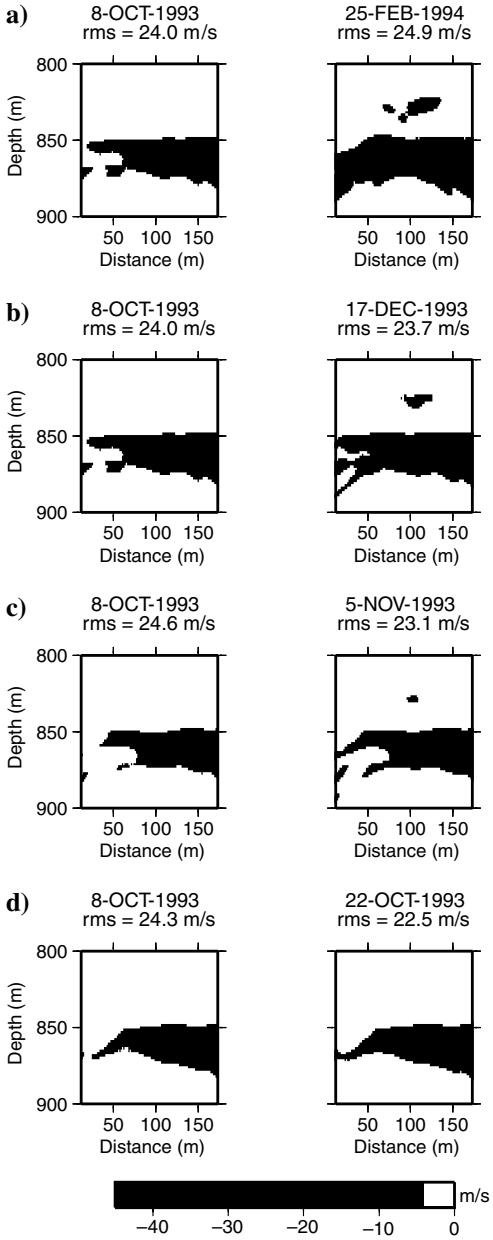

Figure 10. Selected reconstructed velocity-difference models from the data estimated from (a) 10% sparse data sets, (b) 5% sparse data sets, (c) 2% sparse data sets, and (d) 1% sparse data sets. These models are sampled around the beginning of the leak. Because the data space is sampled more frequently in time, the leak is detected earlier with estimated data using 2% sparse data than with the estimated data using 5% or 10% sparse data. Because of the sparsity of the 1% data, the reconstructed velocity models' data do not capture the leaked CO_2.

was executed as a pilot study to monitor changes in the reservoir in response to CO_2 injection into the reservoir. We use data collected between wells JTM-A and JTM-C. In the 1993 survey, JTM-C was the source well and JTM-A was the receiver well. The reverse was the case in the 1995 survey. The wells are separated by about 180 m.

A total of 201 sources and 191 receivers were deployed in the first survey; 200 sources and 192 receivers were deployed in the second survey. Source and receiver intervals were both 1.55 m, and the depth range of the measurements was 678–987 m. The recorded data were rich in frequency bandwidth. The frequency content of the recorded data in the 1993 survey was roughly 350–1500 Hz, sampled at intervals of 0.25 ms, whereas the frequency content of the 1995 data was roughly 350–2000 Hz sampled at intervals of 0.2 ms.

The field data example used here is not an ideal data set on which to test our proposed method. An ideal data set will consist of multiple time-lapse data sets. The choice of the field data example used is based on availability. Also, the time-lapse change in the velocity model is simple. A more complicated time-lapse change in the velocity model would have been preferred.

Conventional time-lapse monitoring

To reconstruct a 2D P-wave velocity model between the two wells, we first pick first-arrival traveltimes. The picks are shown in Figure 12, where the axes of the grids in Figure 12 represent shot and receiver depths. The picking accuracy is about 0.2 ms, one sample point. As expected, we observe the largest traveltime differences at the depths corresponding to the reservoir, caused by a decrease in reservoir seismic velocity from CO_2. Figure 13 shows the difference between the 1993 model and the 1995 model. The reduction in reservoir velocity can be seen in the velocity-difference model.

Time-lapse monitoring with sparse data

After successfully applying the proposed time-lapse monitoring approach to synthetic data, we apply it to the McElroy field data. In this case, we use 5% of the 1995 monitor data set. We selected irregularly spaced traveltimes to obtain the 5% data used. Results are shown in Figure 14. Without data estimation, the reservoir velocity change resulting from the injection of CO_2 is grossly underestimated, as shown in Figure 14b. Using the complete baseline data set and the sparse monitor data set, we estimate the discarded data. The velocity model reconstructed using the estimated data is very

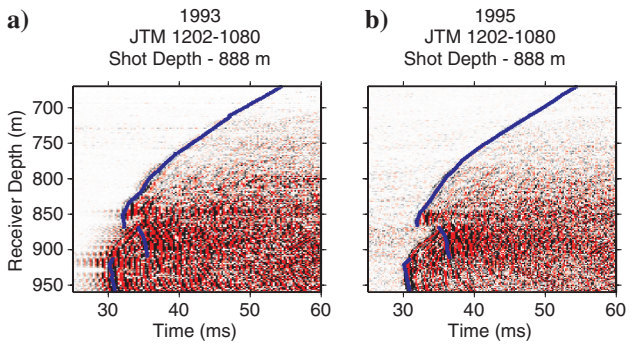

Figure 11. Common-source gathers from the 1993 and 1995 surveys in the McElroy field. The thick, blue curves are direct-arrival traveltimes picked on the gathers.

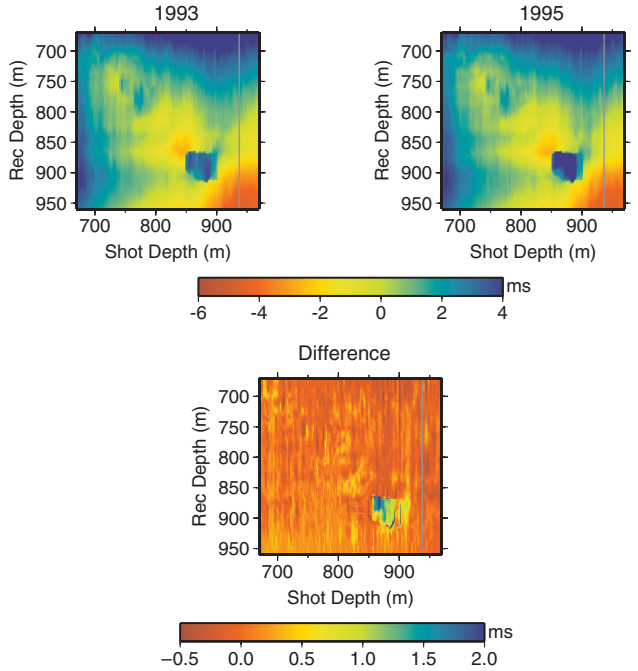

Figure 12. Traveltime data grids picked from the baseline (1993) and monitor (1995) surveys and the difference between the two data sets.

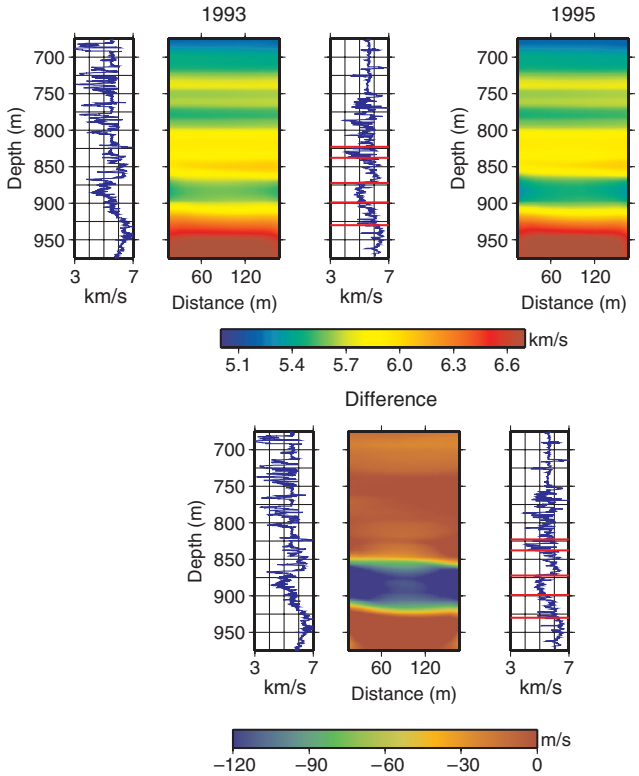

Figure 13. Reconstructed velocity models from the baseline (1993) and monitor (1995) surveys and the velocity-difference model. The 1D velocity logs shown are produced from sonic delta-transit-time well logs. Geologic markers are indicated by horizontal red lines on the logs. There is good agreement between the velocity model and the well logs.

good, as shown in Figure 14c. This result shows the efficiency of the proposed approach for crosswell traveltime field data. An ideal field implementation of our approach will utilize more than two surveys for optimal results.

SUMMARY

To examine the effectiveness of our quasi-continuous monitoring, we created synthetic time-lapse traveltime data sets representative of the field data sets recorded in the McElroy field. The field data were recorded to monitor a reservoir flooded with CO_2 for secondary recovery. We created 70 synthetic time-lapse velocity models representing various modeled states of the field every two weeks from the date of first data acquisition, and we also created their corresponding traveltime data sets. The synthetic models showed CO_2 being injected into the reservoir and leaking into a shallower reservoir 10 months after injection began.

We kept the total size of the monitoring data volume at the end of the surveys constant while varying the size of the sparse data acquired at each time and the length of the time interval between data sets. We used 1%, 2%, 5%, and 10% of the individual complete data sets as our sparse data sets. The data intervals in these data sets were 2, 4, 10, and 20 weeks, respectively. After the unrecorded data sets were estimated, traveltime tomography was used to reconstruct the velocity models. The errors in the reconstructed models were then analyzed.

The synthetic example showed that only a small number of iterations are needed to produce reliable reconstructed velocity models; in our case, only three iterations were needed. As more sparse data sets are acquired, estimates of previously acquired sparse data sets improve in accuracy. The accuracy improves because newer sparse data sets add information to the older data sets.

Because the reconstructed time-lapse models converge after some time, a moving estimation window can be used to reduce computational effort. Furthermore, because total data volume increases with time, once a reconstructed velocity model has stabilized, its data need not be reestimated when new data are available. In the synthetic data example, the CO_2 leak is detected two weeks after it occurred. However, this time delay is much smaller than the conventional time-lapse data acquisition interval.

We also applied the proposed approach to field data. Here, we used the baseline and monitor data from the McElroy Field. We discarded 95% of the monitor data set and then estimated the discarded data from the baseline data and the sparse monitor data. The results show the efficacy of our approach with crosswell traveltime data. With only the baseline and the sparse monitor data set, the reconstructed reservoir velocity change is underestimated. With the baseline and estimated monitor data sets, the reconstructed reservoir velocity change is very close to the true model.

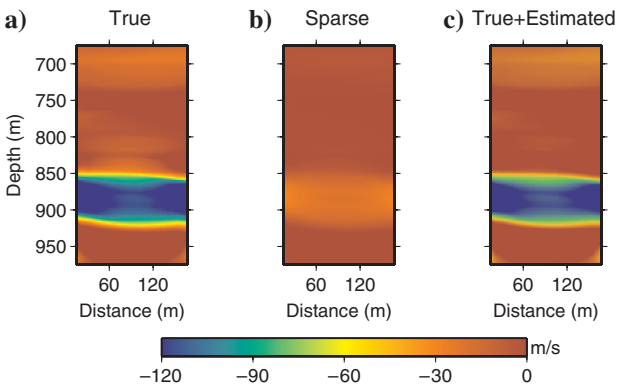

Figure 14. Reconstructed velocity-difference models from (a) the complete field data set, (b) the sparse field data (5% of the complete data set), and (c) 5% sparse + 95% estimated data set.

This paper shows an application of our approach to time-lapse monitoring using 2D crosswell acquisition geometry. In addition, we only considered seismic traveltimes. The conclusions are therefore in reference to crosswell traveltime applications. However, the idea can be extended to 3D surface seismic geometry for time-lapse monitoring, especially if only seismic traveltimes are used. Also, CO_2 sequestration monitoring projects would benefit more from using 3D surface seismic data because of the volumetric coverage provided by 3D geometry.

APPENDIX A

THE ITERATIVE DATA ESTIMATION FORMULATION

A random sequence d_n with zero mean is an autoregressive process of order p when the most recent p outputs and the current input can be used to recursively generate the next output (Jain, 1989). This can be stated as

$$d_n = \sum_{j=1}^{p} g_j d_{n-j} + \varepsilon_n, \tag{A-1}$$

$$E[\varepsilon_n] = 0, \quad E\{[\varepsilon_n]^2\} = \beta^2, \quad E[\varepsilon_n \varepsilon_m] = \beta^2 \delta_{n-m},$$
$$E[\varepsilon_n d_m] = 0, \quad m < n, \tag{A-2}$$

where ε_n is a zero-mean stationary input sequence independent of previous outputs and g_j are the elements of a PEF. Based on only the past p samples, the quantity

$$\hat{d}_n \triangleq \sum_{j=1}^{p} g_j d_{n-j} \tag{A-3}$$

is the optimal linear predictor of d_n (Jain, 1989), which implies

$$d_n = \hat{d}_n + \varepsilon_n. \tag{A-4}$$

Using boldface uppercase letters to represent matrices and boldface lowercase letters to represent vectors, equation A-1 can be written as

$$\boldsymbol{\varepsilon} = \mathbf{D}\mathbf{g} \tag{A-5}$$

or

$$\boldsymbol{\varepsilon} = \mathbf{G}\mathbf{d}, \tag{A-6}$$

respectively (Claerbout, 1998, 2008). The matrix $\mathbf{G}$ contains row-shifted copies of the PEF coefficients vector $\mathbf{g}$, and the matrix $\mathbf{D}$ contains row-shifted copies of the data vector $\mathbf{d}$.

Although data prediction deals primarily with estimating yet-to-be measured data samples from previously measured data samples, data estimation deals with computing missing data samples from an incomplete set of data samples. To estimate missing data using the autoregressive model, equations A-5 and A-6 are satisfied by minimizing the prediction error $\boldsymbol{\varepsilon}$.

Claerbout (1998) suggests a two-stage process for estimating missing data using the PEF. In the first stage, the optimal PEF for the available data is estimated. In the second stage, the estimated PEF is then used to estimate the missing data. Estimating the optimal PEF for an incomplete data set could be done by using a missing-data mask in the estimation process (Claerbout, 1998, 2008) or by using a training data set (Curry, 2008). The PEF is obtained by minimizing the residual $\mathbf{r_d}$:

$$\mathbf{r_d} = \mathbf{DKg} + \mathbf{d} \approx \mathbf{0}, \tag{A-7}$$

where $\mathbf{K}$ is masking operator that ensures that the constrained filter coefficient remains unchanged. These include the zero-lag coefficient of the filter $\mathbf{g}$, which has a value of one. $\mathbf{K}$ is similar to the identity matrix but has a value of zero at positions corresponding to the constrained filter coefficient. Equation A-7 assumes stationarity in the data. Margrave (1998) presents an approach for estimating PEFs for nonstationary data. Here, we solve for a nonstationary PEF of the form

$$\mathbf{f_{ns}} = [\,\mathbf{g}_0 \;\;|\;\; \mathbf{g}_1 \;\;|\;\; \mathbf{g}_2 \;\;|\;\; \cdots \;\;|\;\; \mathbf{g}_n\,]^T, \tag{A-8}$$

with

$$\mathbf{g}_k = [1 - g_{1,k} - g_{2,k} - g_{3,k} \cdots - g_{p,k}]^T,$$

by minimizing the residual,

$$\begin{aligned}\mathbf{0} \approx \mathrm{r_d} &= \mathbf{D}_0\mathbf{K}\mathbf{g}_0 + \mathbf{D}_1\mathbf{K}\mathbf{g}_1 + \cdots + \mathbf{D}_n\mathbf{K}\mathbf{g}_n + \mathbf{d}\\ &= \mathbf{D_{ns}K_{ns}f_{ns}} + \mathbf{d},\end{aligned} \tag{A-9}$$

where $\mathbf{f_{ns}}$ is a nonstationary PEF with the vertical lines separating distinct PEFs; $\mathbf{g}_0, \mathbf{g}_1, \mathbf{g}_2, \ldots, \mathbf{g}_n$ are distinct stationary PEFs; and $\mathbf{D}_k$ contains the subset of $\mathbf{D}$ to be convolved with $\mathbf{g}_k$. The values $\mathbf{D_{ns}}$ and $\mathbf{K_{ns}}$ are nonstationary representations of $\mathbf{D}$ and $\mathbf{K}$, respectively. The objective functions for the least-squares minimization of equation A-9 is

$$\begin{aligned}\boldsymbol{\Phi} &= \|\mathbf{r_d}\|^2 + \alpha^2\|\mathbf{r_r}\|^2\\ &= \|\mathbf{D_{ns}K_{ns}f_{ns}} + \mathbf{d}\|^2 + \alpha^2\|\mathbf{RK_{ns}f_{ns}}\|^2,\end{aligned} \tag{A-10}$$

where $\mathbf{r_r} = \mathbf{RK_{ns}f_{ns}}$, $\alpha^2\|\mathbf{r_r}\|^2$ is a regularization term, $\mathbf{R}$ is a roughening operator, and α is a scaling constant. The regularization term is used to ensure that we obtain a smoothly varying nonstationary PEF.

Minimizing equation A-10 with respect to $\mathbf{f_{ns}}$ and rearranging the terms give

$$\mathbf{f_{ns}} = -(\mathbf{K}_{\mathbf{ns}}^T\mathbf{D}_{\mathbf{ns}}^T\mathbf{D_{ns}K_{ns}} + \alpha^2\mathbf{K}_{\mathbf{ns}}^T\mathbf{R}^T\mathbf{RK_{ns}})^{-1}\mathbf{K}_{\mathbf{ns}}^T\mathbf{D}_{\mathbf{ns}}^T\mathbf{d}. \tag{A-11}$$

After computing the PEF, $\mathbf{f_{ns}}$, the residual of the nonstationary convolution operation is used to estimate the missing data:

$$\begin{aligned}\mathbf{0} \approx \mathbf{r_f} &= \mathbf{G}_0\mathbf{Sd}_0 + \mathbf{G}_0\mathbf{Hd}_0 + \mathbf{G}_1\mathbf{Sd}_1 + \mathbf{G}_1\mathbf{Hd}_1 + \cdots\\ &= \mathbf{F_{ns}Sd} + \mathbf{F_{ns}Hd},\end{aligned} \tag{A-12}$$

where $\mathbf{G}_k$ is a matrix representing convolution with $\mathbf{g}_k$, $\mathbf{d}_k$ is the subset of $\mathbf{d}$ convolved with $\mathbf{g}_k$, $\mathbf{F_{ns}}$ is a matrix representing convolution with $\mathbf{f_{ns}}$, $\mathbf{S}$ can be interpreted to be a data selection operator that selects which data are recorded from the otherwise complete data set, and $\mathbf{H}$ is the difference between the identity operator and $\mathbf{S}$. The value $\mathbf{H}$ selects unknown data; $\mathbf{S}$ selects known data. The objective functions for the least-squares minimization of equation A-12 are

$$\boldsymbol{\Phi} = \|\mathbf{r_f}\|^2 = \|\mathbf{F_{ns}Sd} + \mathbf{F_{ns}Hd}\|^2. \tag{A-13}$$

Minimizing equation A-13 with respect to the data $\mathbf{d}$ and rearranging the terms give,

$$\mathbf{d} = -(\mathbf{H}^T\mathbf{F}_{\mathbf{ns}}^T\mathbf{F_{ns}H})^{-1}\mathbf{H}^T\mathbf{F}_{\mathbf{ns}}^T\mathbf{r}_0 \quad \mathbf{r}_0 = \mathbf{F_{ns}Sd}, \tag{A-14}$$

where $\mathbf{r}_0$ is a constant vector that holds the output of the nonstationary PEF convolved with the known data $\mathbf{Sd}$.

We used an iterative process to estimate unrecorded time-lapse data from recorded time-lapse data. This iterative process can be summarized as follows:

$$\begin{aligned}\mathbf{f}_i^k &= \begin{cases} -(\mathbf{K}^{kT}\mathbf{A}_c^{1T}\mathbf{A}_c^1\mathbf{K}^k + \alpha^2\mathbf{K}^{kT}\mathbf{R}^{kT}\mathbf{R}^k\mathbf{K}^k)^{-1}\mathbf{K}^{kT}\mathbf{A}_c^{1T}\mathbf{a}_c^1 & i = 1 \\ -(\mathbf{K}^{kT}\tilde{\mathbf{A}}_{c,i-1}^{kT}\tilde{\mathbf{A}}_{c,i-1}^k\mathbf{K}^k + \alpha^2\mathbf{K}^{kT}\mathbf{R}^{kT}\mathbf{R}^k\mathbf{K}^k)^{-1}\mathbf{K}^{kT}\tilde{\mathbf{A}}_{c,i-1}^{kT}\tilde{\mathbf{a}}_{c,i-1}^k & i > 1 \end{cases},\\ \tilde{\mathbf{a}}_{c,i}^k &= \mathbf{a}_s^k - (\mathbf{H}^{kT}\mathbf{F}_i^{kT}\mathbf{F}_i^k\mathbf{H}^k)^{-1}\mathbf{H}^{kT}\mathbf{F}_i^{kT}\mathbf{F}_i^k\mathbf{a}_s^k \qquad \forall i,\end{aligned} \tag{A-15}$$

where the subscript i represents iteration number, $\mathbf{f}_i^k$ is the nonstationary filter computed in the ith iteration, $\mathbf{K}^k$ is the constrained filter coefficient masking operator at time k, $\mathbf{R}^k$ is the regularization operator at time k, $\mathbf{a}_c^k$ is the completely sampled accumulated data at time k, $\mathbf{A}_c^k$ is the matrix representing convolution with $\mathbf{a}_c^k$, and $\mathbf{a}_s^k$ is the sparsely sampled accumulated data at time k.

ACKNOWLEDGMENTS

Special thanks go to the Global Climate and Energy Project (GCEP) for supporting this research and the sponsors of the Seismic Tomography Project at Stanford University for providing the field data set used and the permission to publish this work. We would also like to thank the reviewers for their insightful comments and suggestions.

REFERENCES

Ajo-Franklin, J. B., J. Urban, and J. M. Harris, 2005, Temporal integration of seismic traveltime tomography: 75th Annual International Meeting, SEG, Expanded Abstracts, 2468–2472, doi: 10.1190/1.2148222.

Arts, R., O. Eiken, A. Chadwick, P. Zweigel, L. van der Meer, and B. Zinszner, 2004, Monitoring of CO_2 injected at Sleipner using time-lapse seismic data: Energy, **29**, no. 9-10, 1383–1392, doi: 10.1016/j.energy.2004.03.072.

Barkved, O. I., K. Beuer, T. G. Kristiansen, R. M. Kjelstadli, and J. H. Kommedal, 2005, Permanent seismic monitoring of the Valhall Field, Norway: International Petroleum Technology Conference, 10902.

Benson, S. et al. 2005, Underground geological storage, *in* B. Metz, O. Davidson, H. de Coninck, M. Loos, and L. Meyer, eds., IPCC special report on carbon dioxide capture and storage: Cambridge University Press, 195–276.

Claerbout, J. F., 1998, Multidimensional recursive filters via a helix: Geophysics, **63**, 1532–1541, doi: 10.1190/1.1444449.

Claerbout, J. F., 2008, Image estimation by example: Geophysical soundings image construction: Multidimensional autoregression, e-book, accessed 12 March 2008, http://sepwww.stanford.edu/data/media/public/sep//prof/gee.lecture.8.08.pdf.

Clarke, R., O. J. Askim, K. Pursley, P. Vu, and O. J. Askim, 2005, 4D rapid turnaround for permanent 4C installation: 75th Annual International Meeting, SEG, Expanded Abstracts, 2452–2456, doi: 10.1190/1.2148218.

Curry, W., 2008, Interpolation with prediction-error filters and training data: Ph.D. thesis, Stanford University.

Foster, D., S. Fowler, J. McGarrity, M. Riviere, N. Robinson, R. Seaborne, and P. Watson, 2008, Building on BP's large-scale OBC monitoring experience — The Clair and Chirag-Azeri projects: The Leading Edge, **27**, no. 12, 1632–1637, doi: 10.1190/1.3036967.

Harris, J. M., 2004, Geophysical monitoring of geologic sequestration *in* Global Climate and Energy Project 2004 Technical Report, 148–162.

Harris, J. M., R. C. Nolen-Hoeksema, R. T. Langan, M. Van Schaack, S. K. Lazaratos, and J. W. Rector III, 1995, High resolution crosswell imaging of a West Texas carbonate reservoir: Part 1 — Project summary and interpretation: Geophysics, **60**, 667–681, doi: 10.1190/1.1443806.

Harris, J. M., M. D. Zoback, A. R. Kovscek, and F. M. Orr Jr., 2007, Geologic storage of CO_2 *in* Global Climate and Energy Project 2007 Technical Report, 1–98.

Hole, J. A., and B. C. Zelt, 1995, 3-D finite-difference reflection traveltimes: Geophysical Journal International, **121**, 427–434, doi: 10.1111/gji.1995.121.issue-2.

Jain, A. K., 1989, Fundamentals of digital image processing: Prentice-Hall Inc.

Landrø, M., and L. Skopinseva, 2008, Potential improvements in reservoir monitoring using permanent seismic receiver arrays: The Leading Edge, **27**, no. 12, 1638–1645, doi: 10.1190/1.3036968.

Landrø, M., O. A. Solheim, E. Hilde, B. O. Ekren, and L. K. Strønen, 1999, The Gullfaks 4D seismic study: Petroleum Geoscience, **5**, no. 3, 213–226, doi: 10.1144/petgeo.5.3.213.

Lazarotos, S. K., and B. P. Marion, 1997, Crosswell seismic imaging of reservoir changes caused by CO_2 injection: The Leading Edge, **16**, 1300–1306, doi: 10.1190/1.1437788.

Li, C., and R. Nowack, 2004, Application of autoregressive extrapolation to seismic tomography: Bulletin of the Seismological Society of America, **94**, 1456–1466.

Lumley, D., 2001, Time-lapse seismic reservoir monitoring: Geophysics, **66**, 50–53, doi: 10.1190/1.1444921.

Margrave, G. F., 1998, Theory of nonstationary linear filtering in the Fourier domain with application to time-variant filtering: Geophysics, **63**, 244–259, doi: 10.1190/1.1444318.

Mathisen, M. E., A. A. Vasiliou, P. Cunningham, J. Shaw, J. H. Justice, and N. J. Guinzy, 1995, Time-lapse crosswell seismic tomogram interpretation: Implications for heavy oil reservoir characterization, thermal recovery process monitoring, and tomographic imaging technology: Geophysics, **60**, 631–650, doi: 10.1190/1.1443803.

Quan, Y., and J. M. Harris, 2008, Stochastic seismic inversion using both waveform and traveltime data and its application to time-lapse monitoring: 78th Annual International Meeting, SEG, Expanded Abstracts, 1915–1919, doi: 10.1190/1.3059273.

Røste, T., M. Landro, and P. Hatchell, 2007, Monitoring overburden layer changes and fault movements from time-lapse seismic data on the Valhall field: Geophysics Journal International, **170**, no. 3, 1100–1118, doi: 10.1111/j.1365-246X.2007.03369.x.

Santos, E., and J. M. Harris, 2008, DynaSIRT: A robust dynamic imaging methoapplied to CO_2 sequestration monitoring: 78th Annual International Meeting, SEG, Expanded Abstracts, 4019–4023, doi: 10.1190/1.3255708.

Takanami, T., and G. Kitagawa, 1991, Estimation of the arrival times of seismic waves by multivariate time series model: Annals of the Institute of Statistical Mathematics, **43**, no. 3, 407–433, doi: 10.1007/BF00053364.

Wiprut, D., and M. D. Zoback, 2000, Fault reactivation and fluid flow along a previously dormant normal fault in the northern North Sea: Geology, **28**, 595–598, doi: 10.1130/0091-7613(2000)28<595:FRAFFA>2.0.CO;2.

Zelt, C. A., and P. J. Barton, 1998, 3D seismic refraction tomography: A comparison of two methods applied to data from the Faeroe Basin: Journal of Geophysical Research, **103**, no. B4, 7187–7210, doi: 10.1029/97JB03536.